Diameter modulation of 3D nanostructures in Focused Electron Beam Induced Deposition using local electric fields and beam defocus

Javier Pablo-Navarro[1£], Soraya Sangiao[1,2,3£], César Magén[1,2,3] and José María de Teresa[1,2,3*]

[1] Laboratorio de Microscopías Avanzadas (LMA) - Instituto de Nanociencia de Aragón (INA), Universidad de Zaragoza, 50018 Zaragoza, Spain.

[2] Departamento de Física de la Materia Condensada, Universidad de Zaragoza, 50009 Zaragoza, Spain.

[3] Instituto de Ciencia de Materiales de Aragón (ICMA), Universidad de Zaragoza-CSIC, 50009 Zaragoza, Spain.

*Email: deteresa@unizar.es

[£]These authors have equally contributed to the work

Abstract

Focused Electron Beam Induced Deposition (FEBID) is a leading nanolithography technique in terms of resolution and the capability for three-dimensional (3D) growth of functional nanostructures. However, FEBID still presents some limitations with respect to the precise control of the dimensions of the grown nano-objects as well as its use on insulating substrates. In the present work, we overcome both limitations by employing electrically-biased metal structures patterned on the surface of insulating substrates. Such patterned metal structures serve for charge dissipation and also allow the application of spatially-dependent electric fields. We demonstrate that such electric fields can dramatically change the dimensions of the growing 3D nanostructures

by acting on the primary electron beam and the generated secondary electrons. In the performed experiments, the diameter of Pt-C and W-C vertical nanowires grown on quartz, MgO and amorphous SiO_2 is tuned by application of moderate voltages (up to 200 V) on the patterned metal microstructures during growth, achieving diameters as small as 50 nm. We identify two competing effects arising from the generated electric fields: a slight change in the primary beam focus point and a strong action on the secondary electrons. Beam defocus is exploited to achieve the in-situ modulation of the diameter of 3D FEBID structures during growth.

Keywords: focused electron beam induced deposition, three-dimensional nanostructures, nanowires, nanolithography, electrically-biased growth.

1. Introduction

One of the prominent properties searched by any lithography technique is the capability to be used on an arbitrary substrate. In the case of lithography techniques based on charged particles, such as electron beam lithography (EBL) and focused ion beam (FIB) lithography, a limiting factor is the difficulty of working on insulating substrates [1][2]. The building of electric fields in the vicinity of an insulating substrate (due to charging effects) produces unwanted beam deflections that ruin the resolution or even impede their practical application [3][4][5]. In the case of EBL, the problem can be circumvented by working under critical-energy conditions [6], using variable-pressure EBL [7], or including additional steps in the process, like the evaporation of a metal layer on top of the resist that is subsequently etched away [8]. In the case of FIB, it has been found that using electron irradiation simultaneously is helpful towards charge minimization [9].

Focused Electron Beam Induced Deposition (FEBID) is another charged-particle nanolithography technique suffering from the same problem when applied on insulating substrates. FEBID is

capable of nanometer-scale resolution for the growth of two-dimensional [10] and three-dimensional structures [11], and relies on the decomposition of a precursor gas adsorbed on a substrate through the application of a finely-focused electron beam [12][13][14][15]. The FEBID technique is applied for circuit edit and mask repair [16], creation of electrical contacts [17], growth of magnetic nanowires [18][19], fabrication of plasmonic nanostructures [20][21], photodetection [22], gas sensing [23], etc., thus being an important lithography technique in Nanotechnology [24] and Materials Science [25]. In general, these applications are developed using substrates allowing the charge dissipation and the avoidance of detrimental electric potentials in the proximity of the substrate's surface. In fact, we have recently shown that the use of an insulating substrate (such as polycarbonate) hampers the growth of high-resolution nanostructures by FEBID unless pads for charge dissipation exist on the substrate, close to the area of growth [26]. In the present work, we introduce a general strategy to overcome the charging problem in FEBID, consisting on the use of patterned metal structures fabricated by optical lithography or by any other lithography technique. Moreover, if the patterned metal structure on an insulating substrate is electrically biased, large local electric fields can be created on the substrate's surface, producing a tremendous impact on the trajectories of the primary electrons and the generated secondary electrons. We will show that this new degree of freedom in FEBID is useful to tune the dimensions of 3D nanostructures grown by this technique. Previous proof-of-concept work has shown that an electric field produced by a continuous metallic substrate can modify the dimensions of FEBID deposits grown on its surface [27]. Instead, our work focuses on patterned metallic structures with micrometric holes, which allows the application of tunable high electric fields inside the holes and the FEBID growth on insulating substrates.

In our study, we identify two competing effects arising from the generated electric fields: a slight change in the primary beam focus point and a strong action on the secondary electrons. These findings are first exploited to grow out-of-plane FEBID nanowires on insulating substrates with diameter down to 50 nm. Secondly, the growth of 3D FEBID structures with variable diameter is achieved by in-situ tuning of the beam focus. Although the dimension broadening effect of beam

defocus was reported in FEBID [28], in-situ control of this parameter to obtain 3D structures with tailored varying diameters represents a new avenue in the use of FEBID for the growth of functional magnetic, superconducting or photonic materials.

2. Methods

The Pt-C and W-C nanostructures were grown in the commercial Helios Nanolab 650 Dual Beam system equipped with a Schottky field emission gun (S-FEG) electron column and a gas injector system (GIS). The deposits were fabricated selecting an electron beam voltage of 30 kV, an electron beam current of 25 pA and a chamber growth pressure of 1×10^{-5} mbar (base pressure of 2×10^{-6} mbar). The growth pattern was a single circle, continuously scanned by the electron beam for 211 seconds and 60 seconds for Pt-C vertical nanowires, and for 175 seconds for W-C ones. FEBID experiments have been performed using various insulating substrates (MgO, quartz and amorphous SiO_2) in order to verify that the observed behaviour is general for non-conductive systems and cannot be attributed to one particular type of substrate. The tested precursors are $(CH_3)_3Pt(CpCH_3)$ for Pt-C deposition [29] and $W(CO)_6$ for W-C deposition [30]. As expected, bare insulating MgO and quartz substrates did not allow the growth of Pt-C or W-C vertical nanowires, due to the presence of large and uncontrolled electric fields on the substrate surface that affect dramatically the trajectory of the incoming electron beam and the secondary electrons generated at the substrate. In the case of growth of vertical nanowires by FEBID, charging effects are expected to be very important because the electron irradiation point is fixed, and most of the charges accumulate in the substrate, below and in the proximity of the nanowire's standing point. As shown in Figure S1 in the Supplementary File, it was found that no nanowire could be grown on MgO and quartz substrates, in contrast to the use of 300 nm-thick amorphous SiO_2 substrate on Si, where charge dissipation is possible via the Si substrate.

Our strategy to avoid charging effects during the growth of vertical nanowires by FEBID is

sketched in Figure 1. Optical lithography has been used to pattern a periodic array of holes in a Cu thin layer grown on top of the insulating substrate (other lithography techniques and/or metal could have been used). The 500 nm Cu film is perforated with circular holes of diameter ~4 μm. The importance of the shape and dimension of the holes will be later discussed.

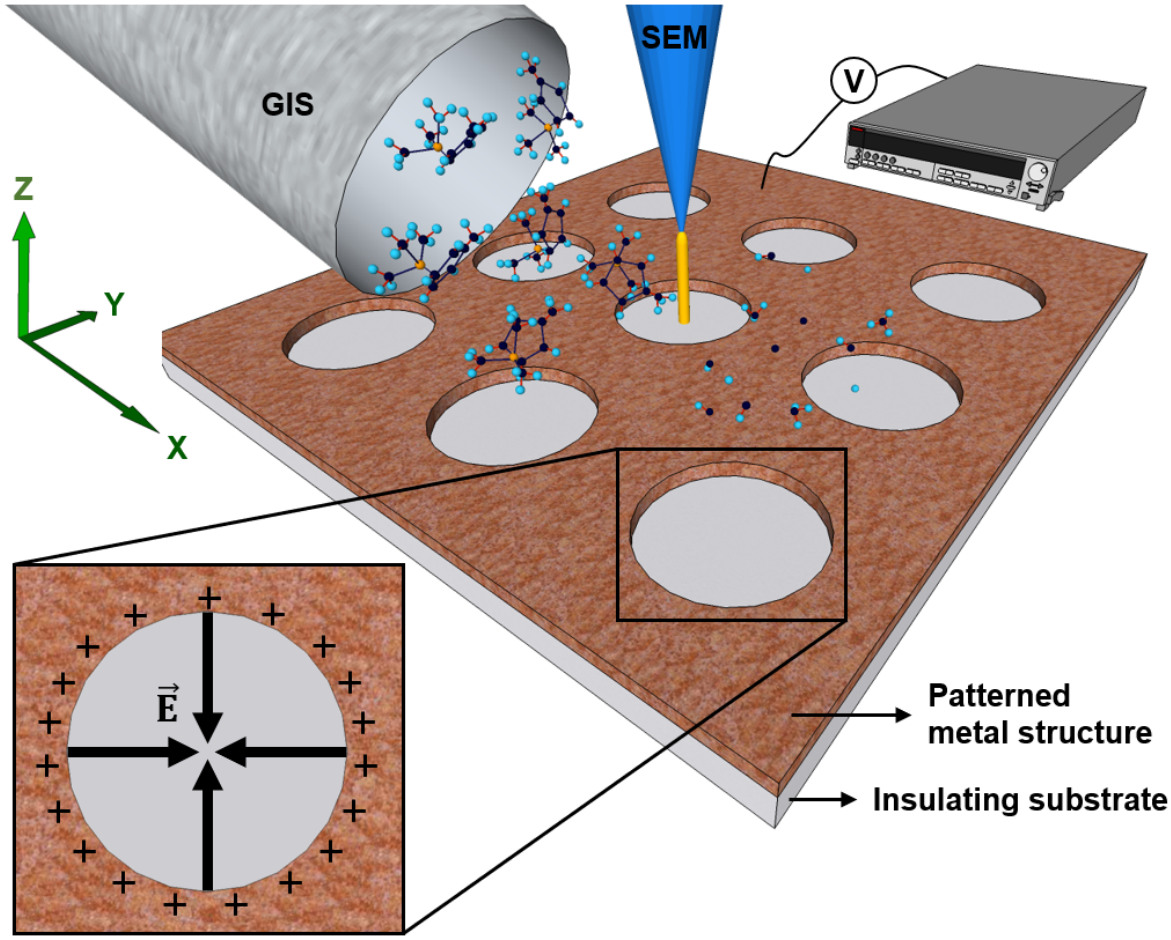

Figure 1. Sketch illustrating the FEBID process carried out on an insulating substrate with an electrically-biased patterned metal structure in order to tune the dimensions of three-dimensional nanostructures by application of local electric fields.

3. Results and discussion

The growth of the Pt-C nanowires has been performed following the method described in section 2. A continuous electron irradiation on the point of interest, whilst the precursor is flowing, gives rise to the growth of out-of-plane nanowires. The current understanding of the growth process implies that the growth rate primarily depends on the electron current, the efficiency of the primary and generated secondary electrons for precursor dissociation, and on the precursor availability, which depends on the direct precursor flux arriving to the place of growth as well as on the precursor diffusion from the substrate. During the growth process, electric fields can *a priori* be relevant in two ways: the build-up of uncontrolled electric fields due to charging effects can hamper the nanowire's growth and the use of controlled electric fields can modify the trajectories of the primary and secondary electrons, enhancing the efficiency of the precursor dissociation. The use of the perforated Cu layer has been found to be efficient to evacuate the charge produced during the nanowires' growth, as particularly shown in Figure 2. In this figure, it can be noted that there is no difference between performing the growth on the copper layer itself and on an insulating MgO substrate, in the centre of a hole perforated on the Cu layer. In both cases, a Pt-C nanowire grows with diameter of 70 nm and similar length. This means that charging effects are avoided with this strategy.

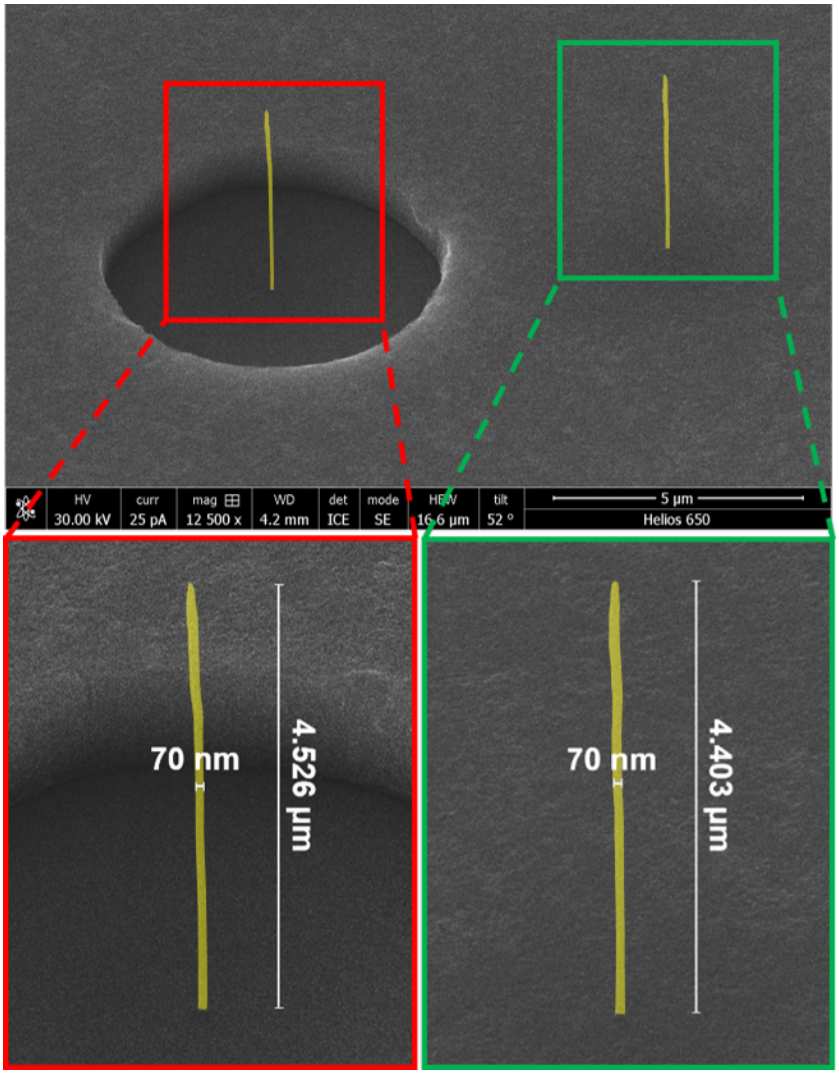

Figure 2. SEM micrographs obtained after 211 s of growth of Pt-C vertical nanowires on an insulating MgO substrate (red frame) at the centre of a 4-µm-diameter hole of the perforated copper layer and onto the copper layer (green frame). The nanowires have been artificially coloured (the original images can be seen in the Supplementary File, Figure S2).

Additionally, Figure 1 illustrates the possibility of getting benefit from an additional degree of freedom: the application of an electric potential to the perforated Cu layer. For that, an external voltage source is used to provide a voltage difference between the Cu layer and the electrical ground of the system, which coincides with that of the sample holder. A cable connects the external source to the sample holder through a chamber feedthrough and a microwire is bonded

between the sample holder and the Cu perforated layer. This source allows applying DC voltages from -200 V to +200 V. As a consequence, large variations in the local electric fields are produced inside and around the holes of the perforated Cu layer, as shown in Figure 3.

In order to quantitatively describe the electric field produced by the perforated metallic structure, here we calculate the total electric field in the vicinity of a circular hole, using the superposition principle. The total electric field is calculated as the field due to an infinite sheet (without the hole) minus the field due to a disk of the same size as the circular hole, considering that both, sheet and disk, carry the same surface charge density, σ, generated through the application of an electric potential. The radial, $E_{r,\,disk}$, and axial, $E_{z,\,disk}$, field as a function of the distance from the symmetry axis of an uniformly-charged circular disk of radius R can be calculated using the following expressions [31]:

$$E_{r,\ disk} = \frac{\sigma}{2\,\pi\,\varepsilon_0}\left[\frac{\delta}{\beta}\big(K(k) - E(k)\big) - \frac{2}{\delta}K(k)\right]$$

$$E_{z,\ disk} = \frac{\sigma}{2\ \varepsilon_0}\left[a' + b'\beta^2 + c'\beta^4 + d'\beta^6\right]$$

Where $\delta^2 = 1 + \alpha^2 + \beta^2 + 2\beta$, $\alpha = {}^{z}/_{R}$, $\beta = {}^{r}/_{R}$, $k = {}^{2\sqrt{\beta}}/_{\delta}$, ε_0 is the vacuum permittivity, K(k) and E(k) are complete elliptic integrals of the first and second kind, respectively, and $a' = 1 - \frac{\alpha}{(1+\alpha^2)^{1/2}}$, $b' = -\frac{3}{4}\frac{\alpha}{(1+\alpha^2)^{5/2}}$, $c' = -\frac{15}{64}\frac{3\alpha - 4\alpha^3}{(1+\alpha^2)^{9/2}}$, $d' = -\frac{45}{2304}\frac{35\,\alpha - 140\,\alpha^3 + 56\,\alpha^5}{(1+\alpha^2)^{13/2}}$. Figure 3 shows the resulting numerical calculations of the electric field in the vicinity of a circular hole of 2 microns in radius in two different planes of the patterned metallic structure. The vector map of the electric field inside the hole, xy plane in Figure 1, is displayed in Figure 3(a), which illustrates that the application of a negative (positive) DC voltage in such structure produces large and highly directional electric fields pointing towards (or from) the centre of the hole. In the centre of the hole, the electric field vanishes. The total electric field in the plane perpendicular to the hole, xz plane in Figure 1, corresponds to the vector map shown in Figure 3(b). The electric field is very small along the symmetry axis of the circular hole and

grows rapidly as the distance from this axis increases.

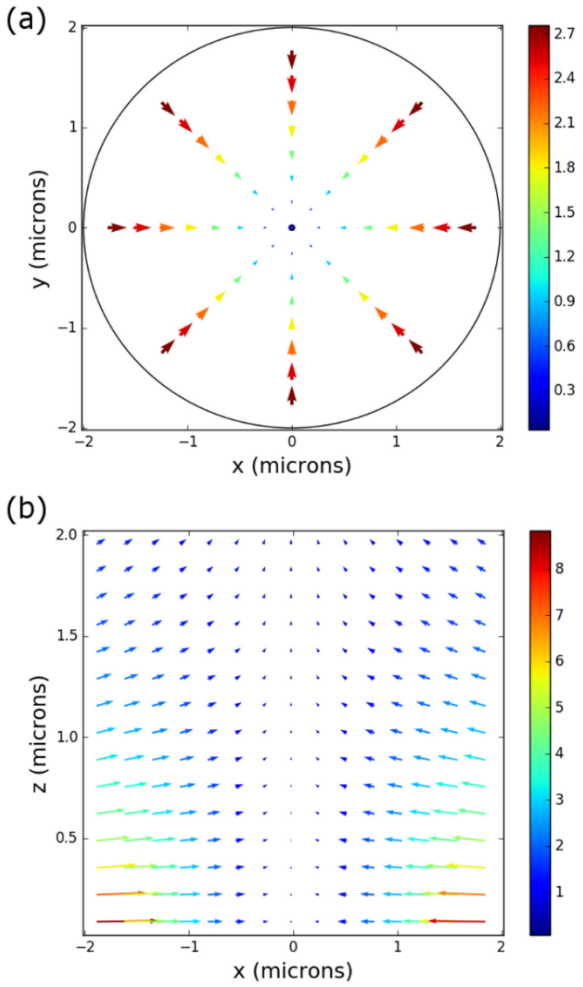

Figure 3. Numerical calculations of the electric field in the vicinity of a circular hole of 2 microns in radius in two different planes of the patterned metallic structure, produced by the application of a negative voltage to the chip: (a) Electric field in the hole plane, xy plane in Figure 1, at a distance z = 1 micron and (b) electric field in the plane perpendicular to the hole, xz plane in Figure 1, containing the vertical symmetry axis of the hole. Electric field values are expressed in units of $\sigma / (2\ \varepsilon_0)$.

It has been observed that the growth of the nanowires under different voltage values applied to the perforated metal layer, whilst keeping constant the other growth conditions, affects dramatically the dimensions of the nanowires, as shown in Figure 4. In these experiments all the

Pt-C nanowires are grown at the centre of the 4-μm-diameter holes of a perforated Cu film with amorphous SiO_2 substrate. Experiments were carried out by growing nanowires under various voltages in the -200 V to +200 V range. The deposition time has been chosen to grow nanowires with maximum length of 3 μm, given that longer nanowires can suffer from precursor depletion and beam drift, as well as variations in the electric field along their height, as shown in Figure 3. As shown in Figure 4(a), the nanowire's diameter is found to change from a large value around 100 nm under -200 V to a minimum value of 50 nm at -25 V, increasing again to 90 nm under +200 V. This figure illustrates the tuning of the value of the nanowire's diameter in a factor of 2 by application of the local electric fields created. The aspect ratio of the nanowire, defined as the quotient between the length (L) and the diameter (ϕ), is also represented in Figure 4(a). It shows a maximum value around -25 V, in good correspondence with the minimum value of the diameter at such voltage, and indicates that the aspect ratio increases a factor of 4 working under such voltage in comparison to -200 V. SEM micrographs of three Pt-C nanowires grown respectively under voltages of -100 V, -35 V, and +100 V are shown in Figure 4(b), 4(c) and 4(d). In the first case, under -100 V, the diameter at 1 μm height is 73 nm, whereas it decreases to 50 nm under -35 V and increases again to 83 nm under +100 V. Moreover, the nanowire's length is respectively at those voltages 2.6 μm (-100 V), 2.9 μm (-35 V) and 2.2 μm (+100 V), corresponding to linear growth rates of 43.3 nm/s, 48.3 nm/s, and 36.7 nm/s, respectively. Thus, the results are conclusive with respect to an optimized nanowire growth in terms of resolution under negative voltages around -25 V.

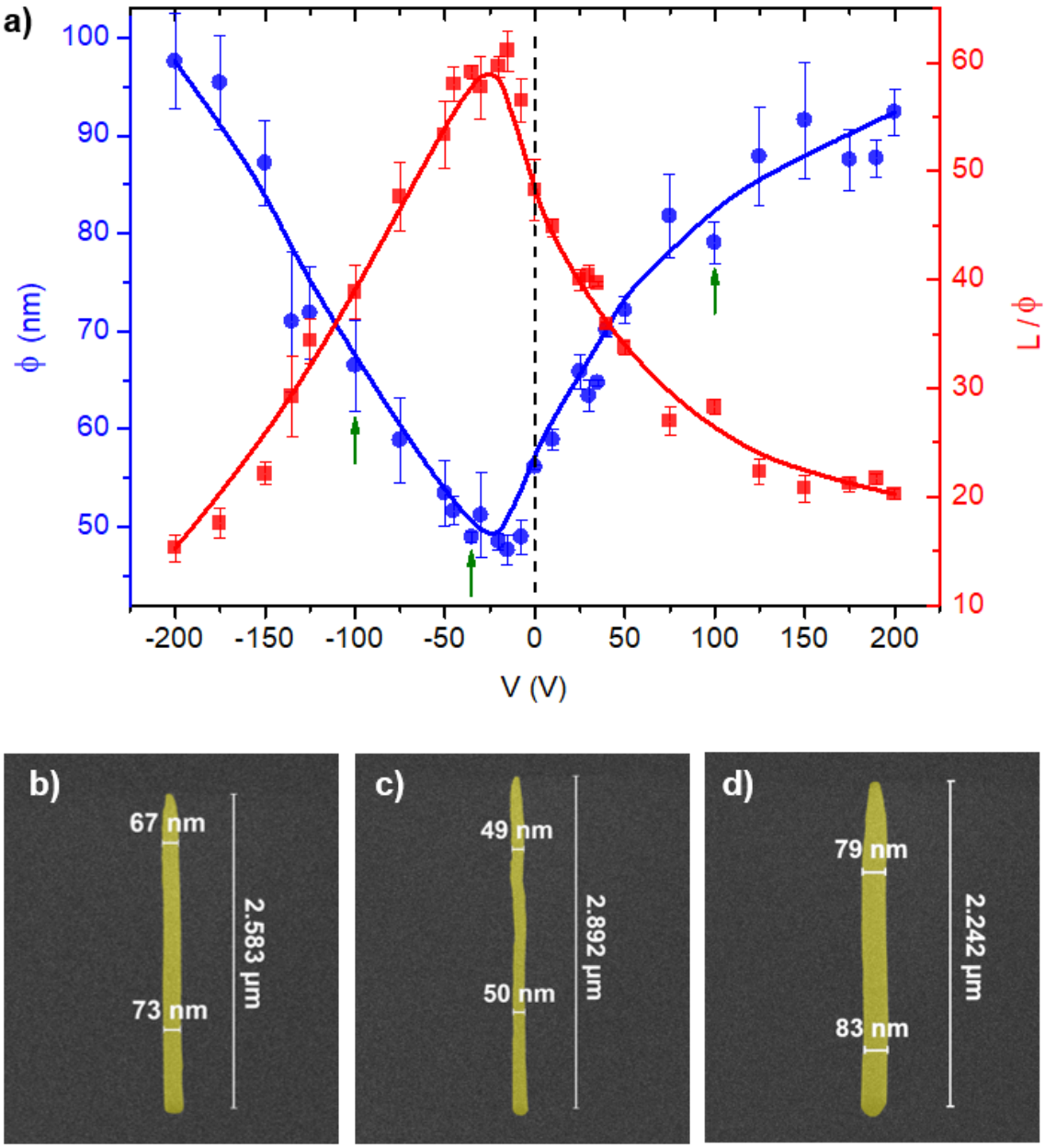

Figure 4. For Pt-C nanowires grown for 60 s on amorphous SiO_2 substrate, (a) dependence of their diameter and the ratio between their length and diameter with the voltage applied to the perforated metallic structure. Each data point represents the average value after measurements of several nanowires grown under the same conditions and at various locations in each nanowire. The lines are visual guides. SEM micrographs of selected nanowires grown under an external voltage of (b) -100 V, (c) -35 V, (d) +100 V. The nanowires have been artificially coloured (the original images can be seen in the Supplementary File, Figure S3) and correspond to the points marked with green arrows on (a).

Similar experiments have been carried out to investigate the influence of local electric fields on the dimensions of W-C nanowires grown by FEBID using a perforated Cu film on the same amorphous SiO_2 substrate by means of the $W(CO)_6$ precursor. As shown in the Supplementary File (Figure S4), the minimum nanowire's diameter (65 nm) occurs in the voltage range -25 V to -50 V and the aspect ratio is maximized in the same voltage range. In this case, the degree of tunability of the diameter and the aspect ratio, compared to the Pt-C case, is lower but substantial (a factor of 1.3 and 1.7 respectively). The set of results obtained for Pt-C and W-C nanowires are thus conclusive to establish spatially-dependent electric fields as a new degree of freedom to tune the dimensions of nanowires grown by the FEBID technique. The origin of the effect will be discussed hereafter in the light of the physical phenomena involved in the FEBID growth and the electric field distribution around the perforated metallic structure (calculations shown in Figure 3).

Regarding the physical phenomena involved in the growth of vertical structures by FEBID, Fowlkes et al. noted that the most significant contribution to the dissociation of the precursor molecules arises from electrons in the primary beam (PE) and their generated secondary electrons (SE-I), with lower relevance from backscattered electrons (BSE) and their generated secondary electrons (SE-II) [32]. Later, Smith et al. stressed the important role played by forward-scattered electrons (FSE) in the growth of pillars as well as the dependence of the effect with the primary beam energy and the resulting growth regime [33]. Moreover, Arnold et al. showed that SE-II electrons are responsible for the halo deposit around the main deposit in two-dimensional deposits, affecting the final deposit resolution [34]. A similar study by Schmied et al., but for three-dimensional deposits, has shown various competing effects, with significant broadening of the deposit width under intermediate or low electron beam energy [35]. The FEBID process is thus complex and depends on many parameters, but in general the precursor dissociation process is determined by high-energy electrons (mainly arising from PE and FSE) as well as by low-energy electrons (mainly SE-I but also SE-II). As a consequence, our experimental finding of a large effect of local electric fields on the dimensions of FEBID deposits should be correlated with

the effect produced by such electric fields on the trajectories of these electrons responsible for the precursor dissociation. In the following, we provide a qualitative explanation of the observed effect, which is sketched in Figure 5.

We put forward that the perforated Cu film is in fact acting as a small electrostatic lens. Electrostatic lenses can be found in electron/ion microscopes [36] and other devices based on charged particles [37] with the aim of focusing or defocusing a charged beam. In our case, as the primary electron beam approaches the perforated charged film, it suffers a deviation towards the optical axis (negative voltage) or off the optical axis (positive voltage), as sketched in Figure 5. In both cases, this effectively leads to an electron beam defocus. As reported by Plank et al. [28], the effect of defocusing the primary electron beam leads in FEBID to an increase of the nanowire's diameter. On the other hand, the high electric field will strongly modify the trajectory of the secondary electrons [27], which are also crucial for the FEBID growth, as discussed above. Due to the low energy of SE-I and SE-II electrons (< 50 eV range) [38], they will undergo strong attraction or repulsion towards the optical axis for negative or positive voltage respectively. In fact, similar voltage values in the range of a few tens or hundreds of volts are actually used in electron microscopes to optimize the imaging contrast by secondary electrons, where biasing voltage can be applied to the sample itself [39][40], or to the electron detector [41][42]. In our application, the use of a negative voltage will push SE-I and SE-II electrons to the hole centre of the patterned metallic film, contributing to decrease the nanowire's diameter. Summarizing, when a negative voltage is applied to the perforated Cu film, two effects will compete: nanowire narrowing due to the effect of the electric field on the SE-I and SE-II electrons and nanowire broadening due to the defocusing effect of the electric field on the PE electrons. This is in agreement with the experimental results, shown in Figure 4 and Figure S4. Starting from 0 V, the nanowire diameter first decreases down to an applied voltage around -30 V, to increase again down to -200 V. As the sketch in Figure 5 illustrates, this is the expected evolution given the rapid focusing of the secondary electrons towards the hole centre at low voltages and the smoother increase of the primary beam diameter with the voltage. At positive voltage, the diameter is

always increasing with voltage given that both effects contribute to the nanowire broadening.

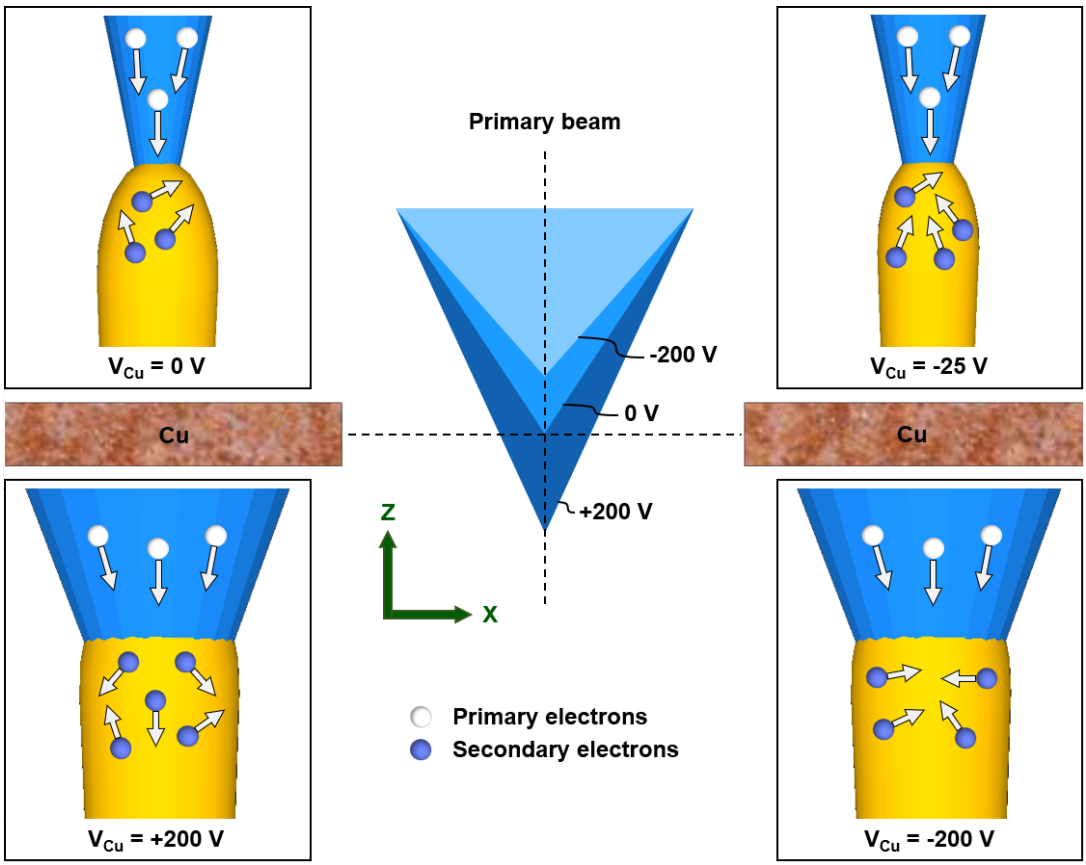

Figure 5. Sketch illustrating the relevant phenomena involved in the growth of pillars by FEBID when an external positive or negative voltage is applied to a patterned metallic layer on top of the substrate. On the one hand, the primary beam becomes slightly defocused by application of positive or negative electric fields, giving rise to the nanowire broadening. On the other hand, the secondary electrons produced in the substrate and the growing structure will be strongly attracted to or repelled from the central optical axis, depending on the negative or positive sign of the applied voltage and contributing respectively to the nanowire narrowing or broadening.

In order to verify this hypothesis, additional experiments were performed where the electron beam focus conditions were controllably changed during the nanowire growth. For that, the focus height (z) was varied with respect to the optimum focus condition in order to investigate the corresponding changes in the nanowire diameter and height. The experiments consisted of the

growth of more than fifty Pt-C nanowires for 60 s on the amorphous SiO_2 substrates for different z values. The obtained results for the values of the diameter and length/diameter ratio are represented in Figure 6. In order to check that the broadening effect is independent of the voltage applied to the patterned metal layer, the experiments were performed at -25 V and at -200 V, respectively represented in Figure 6(a) and 6(b). The z value has been typically swept between -20 μm and 20 μm, which leads to enormous differences in the nanowire's diameter (up to a factor of 3) and in the length/diameter ratio (up to a factor of 12).

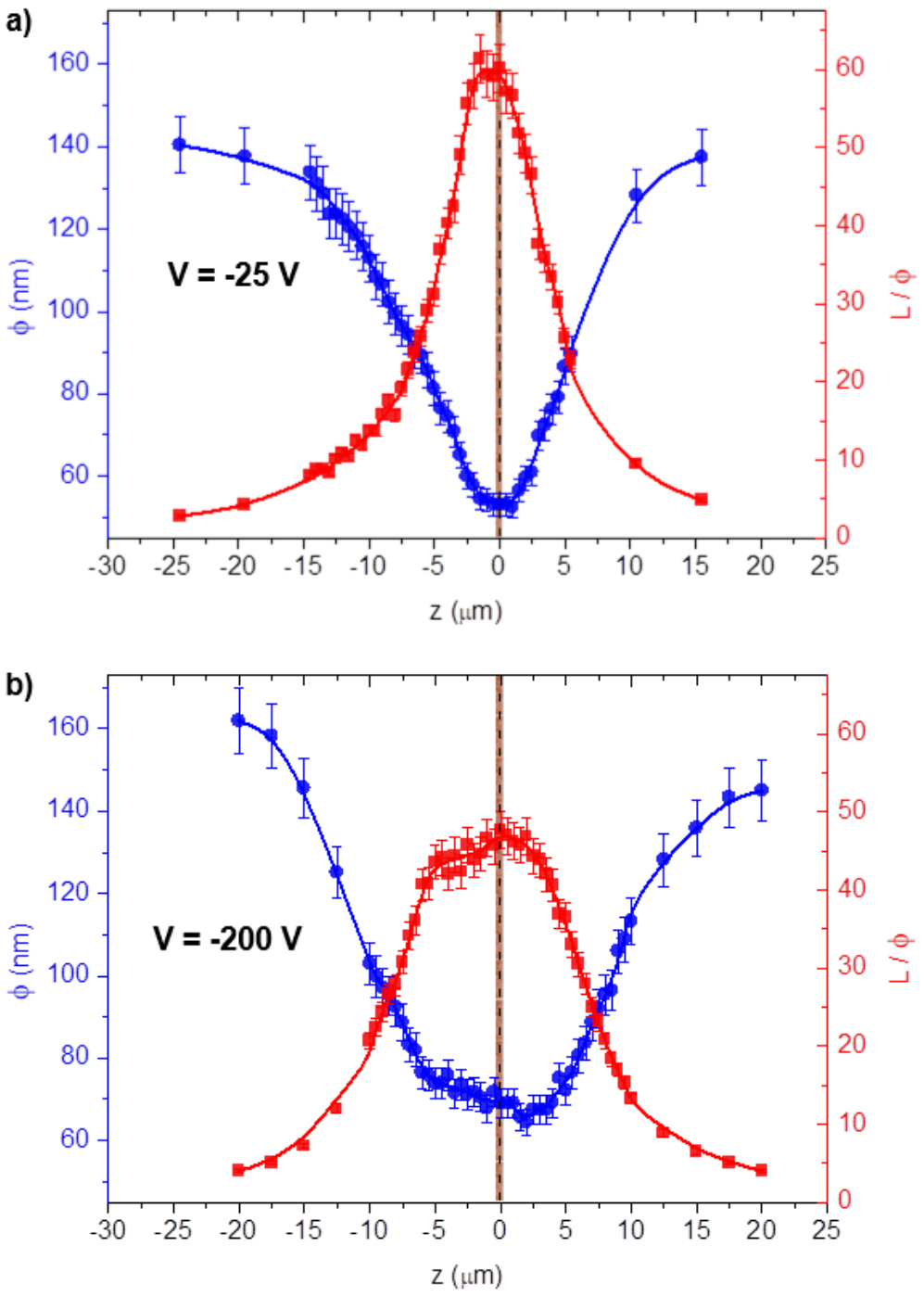

Figure 6. For Pt-C nanowires grown on SiO_2 for 60 s under the same conditions, dependence with the primary beam focus height of the diameter at half nanowires' height and the ratio between their length and diameter. In these experiments, the voltage applied to the patterned metal layer was respectively (a) -25 V and (b) -200 V. Each data point represents the average value after measurements of several nanowires grown under the same conditions and at various locations in each nanowire. The lines are visual guides.

These results highlight, on the one hand, the importance of a good primary beam focus in order to reach the highest resolution in the growth of three-dimensional nanostructures. In order to show which differences appear in the SEM images when the z value varies in the -20 μm to 20 μm range, an example is shown in Figure S5 in the Supplementary File. On the other hand, the results interestingly show an additional degree of freedom to play with during the growth of three-dimensional nanostructures by FEBID. In order to exploit this additional parameter, we have varied the z value during the growth of single nanowires in order to create nanowires with modulated diameter. First, as shown in the left part of Figure 7, a Pt-C nanowire with large diameter (146 nm) starts to grow on the amorphous SiO_2 substrate due to the primary beam defocus (z value of 20 μm out of focus). But, at 72 s, by bringing the sample into focus with a quick (in about 1 s) change in the z position, a narrow section (64 nm in diameter) starts to grow. After another 72 s, we again modify the z position 20 μm, producing a primary beam defocus and the corresponding increase of the nanowire's diameter to 119 nm. After 72 s growth in these conditions, the growth is terminated, leaving a diameter-modulated nanowire with large-narrow-large sections. A second diameter-modulated nanowire has been grown following a similar strategy but with narrow-large-narrow sections, as shown in Figure 7 on the right. This strategy to in-situ modulate the nanowire's diameter based on beam defocus should in principle work on any metal substrate. However, the use of a perforated metal layer allows the growth of modulated nanowires on insulating substrates and provides further diameter modulation through the use of the applied voltage.

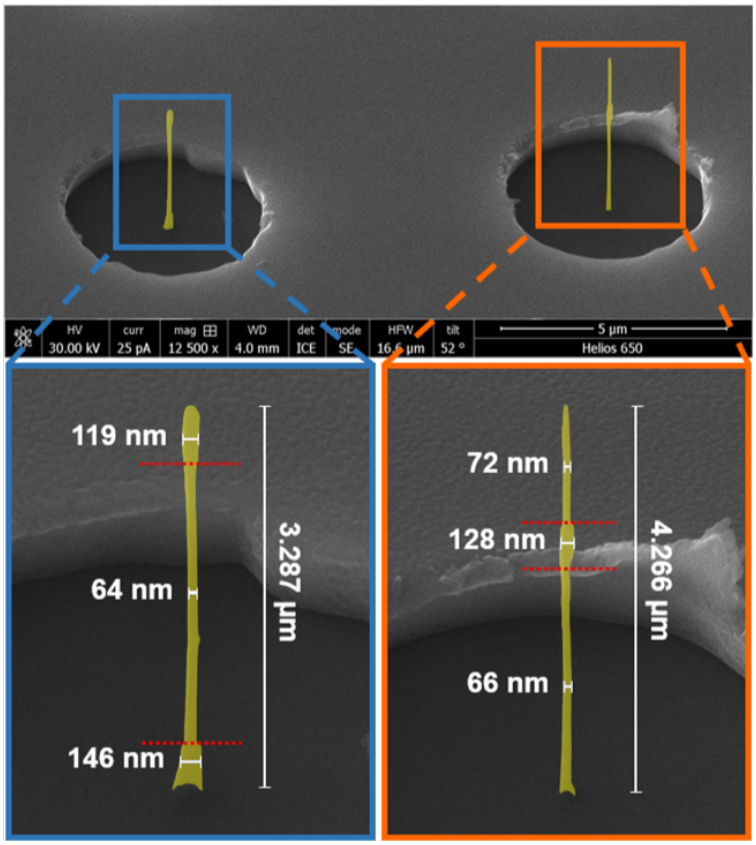

Figure 7. Pt-C nanowires with modulation of diameter, grown on SiO_2 by means of the in-situ variation of the primary electron beam focus condition. Each thin and thick diameter region in the nanowires was fabricated for 72 s, which is marked with dot red lines on the images. The nanowires have been artificially coloured (the original images can be seen in the Supplementary File, Figure S6).

It is interesting to mention that, despite every section in the nanowires of Figure 7 has been grown for 72 s, their respective length is different. This is expected for sections with dissimilar diameter, where one would expect conservation of the volume growth rate instead of the linear growth rate. But it also occurs for sections with the same diameter, which can be explained by the diminishment of the growth rate with an increasing distance to the substrate caused by precursor diffusion effects [19].

4. Conclusions and perspectives

In the current work, we introduce patterned metallic microstructures to allow FEBID growth on insulating substrates and to tune the lateral dimension of three-dimensional nanostructures. In fact, when a voltage is applied to the patterned metallic microstructure, the spatially-dependent electric field generated acts as a small electrostatic lens, affecting the primary and secondary electrons involved in the growth of the nanowires. This new approach has been applied to the growth of Pt-C (and W-C) nanowires, finding that the width and aspect ratio can be changed by a factor of 2 and 4 respectively by application of voltages up to 200 V. These results emphasize the potentiality of spatially-dependent local electric fields to tune the growth of 3D structures by FEBID. The effect of the local electric fields on the primary electron beam has been found to be equivalent to that of a beam defocus, which broadens the diameter of the growing nanostructure. This finding has been applied to the growth of nanowires with modulated diameter in one single step, with either large-narrow-large sections or narrow-large-narrow sections. On the other hand, the local electric fields also attract (repel) the secondary electrons towards (from) the optical axis of the primary beam, producing the shrinkage (broadening) of the growing nanostructure.

In the following, we put forward some perspectives opened by the current results and deserving future exploration.

-One can think over the insertion of perforated metal plates in an automatized way on top of insulating substrates with small gap distance. This would be similar to the automatic insertion of apertures in electron microscopes. In this fashion, and via the application of controlled voltages to such perforated metal plates, an additional and automatized knob for diameter modulation would be available for FEBID growth of three-dimensional nanostructures.

-Although our work here has been focused on metal layers with round holes, different geometries could be given to the holes, thus producing tailored distributions of electric fields. This could be applied to grow 3D structures with asymmetric tailored arms.

-The produced FEBID deposits could be used as hard-mask structures [43] on insulating substrates for subsequent lithography steps where, typically, the insulator is subsequently etched away except on the areas covered by the hard mask. This approach could be competitive with respect to EBL, FIB or other patterning techniques suffering from charging effects.

-The use of electrically-biased patterned layers proposed here could also work for FIBID growth on insulating substrates. In the case of FIBID, the precursor dissociation mechanisms are still under debate [44], but the relevant role of secondary electrons in the growth of pillars has been confirmed [45][46].

-In-situ modification of the applied voltage to the patterned metal film or in-situ change of the focus height could be useful towards the growth of 3D functional nanostructures with varying diameter. As an example, in 3D magnetic nanowires, diameter changes are natural locations for magnetic domain-wall pinning, with applications in magnetic storage and logics [47][48].

- Other possible interesting materials for which this technique could offer advantages are plasmonic materials, such as Au and Ag, and magnetic materials, such as Co and Fe. The growth of core-shell nanowires is also possible in FEBID, which cam be of application for the growth of hybrid materials harnessing multifunctional properties [49].

-The use of a patterned metal layer allows for the growth of one nanowire per hole (as shown in the Supplementary File, Figure S7). Once all the nanowires have been grown, the Cu plate can be etched away by means of an etching solution, which would allow further sample processing. Similar approach is used for graphene grown by Chemical Vapour Deposition on a metal substrate, which is subsequently etched away, and the graphene is transferred to an arbitrary substrate [50].

-Future full-fledged simulations of the electron trajectories (such as Monte Carlo simulations) including the presence of spatially inhomogeneous electric fields, if feasible, could provide a more detailed understanding of the physical phenomena behind the experimental results shown in the current work.

In summary, tuning of nanowire dimensions during FEBID growth has been demonstrated by the use of controlled voltage applied to a patterned metal layer on top of the substrate. The use of spatially-dependent electric fields on the substrate represents a new degree of freedom for the growth of tailored 3D nanostructures by FEBID. The local electric fields have been found to act on the trajectories of the primary beam and of the secondary electrons, both contributing to the precursor dissociation and thus to the lateral dimension of the growing nanostructures. In addition, single nanowires with modulated diameter (with either large-narrow-large sections or narrow-large-narrow sections) have been achieved by in-situ acting on the beam defocus, offering a new route to create three-dimensional complex nanostructures with tailored lateral dimensions.

Acknowledgements

Financial support from the Spanish Ministry of Economy and Competitiveness through the projects MAT2017-82970-C2-1-R, MAT2017-82970-C2-2-R and MAT2015-69725-REDT, from the Aragon Regional Government (Construyendo Europa desde Aragón) through the project E13_17R with European Social Fund funding is acknowledged. J. P.-N. grant is funded by the Ayuda para Contratos Predoctorales para la Formación de Doctores, Convocatoria Res. 05/06/15 (BOE 12/06/15) of the Secretaría de Estado de Investigación, Desarrollo e Innovación in the Subprograma Estatal de Formación of the Spanish Ministry of Economy and Competitiveness with the participation of the European Social Fund. Experimental help by R. Valero, G. Simón, L. Casado and I. Rivas from the Laboratory of Advanced Microscopies (LMA) is acknowledged.

Author contributions. J. M. D. T. proposed the project, supervised the research and wrote the first version of the manuscript. J. P.-N. and S. S. performed the experimental work, discussed the results and contributed to the manuscript. C. M. discussed the results and contributed to the manuscript. All authors have given approval to the final version of the manuscript.

Competing financial interests. The authors declare no competing financial interests.

ORCID IDs

Javier Pablo-Navarro https://orcid.org/0000-0001-6771-6941

Soraya Sangiao https://orcid.org/0000-0002-4123-487X

César Magén https://orcid.org/0000-0002-6761-6171

José María De Teresa https://orcid.org/0000-0001-9566-0738

References

[1] Satyalakshmi K M, Olkhovets A, Metzler M G, Harnett C K, Tanenbaum D M and Craighead H G 2000 Charge induced pattern distortion in low energy electron beam lithography *J. Vac. Sci. Technol. B Microelectron. Nanom. Struct.* **18** 3122

[2] Menard L D and Ramsey J M 2011 Fabrication of sub-5 nm nanochannels in insulating substrates using focused ion beam milling *Nano Lett.* **11** 512–7

[3] Cazaux J 1986 Some considerations on the electric field induced in insulators by electron bombardment *J. Appl. Phys.* **59** 1418–30

[4] Toth M, Knowles W R and Thiel B L 2006 Secondary electron imaging of nonconductors with nanometer resolution *Appl. Phys. Lett.* **88** 023105

[5] Li W Q, Mu K and Xia R H 2011 Self-consistent charging in dielectric films under defocused electron beam irradiation *Micron* **42** 443–8

[6] Joo J, Chow B Y and Jacobson J M 2006 Nanoscale patterning on insulating substrates by critical energy electron beam lithography *Nano Lett.* **6** 2021–5

[7] Myers B D and Dravid V P 2006 Variable pressure electron beam lithography (VP-eBL): A new tool for direct patterning of nanometer-scale features on substrates with low electrical conductivity *Nano Lett.* **6** 963–8

[8] Cumming D R S 1997 Efficient diffractive optics made by single-step electron beam lithography in solid PMMA *J. Vac. Sci. Technol. B Microelectron. Nanom. Struct.* **15** 2859

[9] Stokes D J, Vystavel T and Morrissey F 2007 Focused ion beam (FIB) milling of electrically insulating specimens using simultaneous primary electron and ion beam irradiation *J. Phys. D. Appl. Phys.* **40** 874–7

[10] Ven Kouwen L, Botman A and Hagen C W 2009 Focused electron-Beam-induced deposition of 3 nm dots in a scanning electron microscope *Nano Lett.* **9** 2149–52

[11] Fowlkes J D, Winkler R, Lewis B B, Stanford M G, Plank H and Rack P D 2016 Simulation-Guided 3D Nanomanufacturing via Focused Electron Beam Induced Deposition *ACS Nano* **10** 6163–72

[12] Utke I, Hoffmann P and Melngailis J 2008 Gas-Assisted Focused Electron Beam and Ion Beam Processing and Fabrication *J. Vac. Sci. Technol. B Microelectron. Nanom. Struct.* **26** 1197–276

[13] Van Dorp W F and Hagen C W 2008 A critical literature review of focused electron beam induced deposition *J. Appl. Phys.* **104** 081301

[14] Randolph S J, Fowlkes J D and Rack P D 2006 Focused, Nanoscale Electron-Beam-Induced Deposition and Etching *Crit. Rev. Solid State Mater. Sci.* **31** 55–89

[15] Huth M, Porrati F, Schwalb C, Winhold M, Sachser R, Dukic M, Adams J and Fantner G 2012 Focused electron beam induced deposition: A perspective *Beilstein J. Nanotechnol.* **3** 597–619

[16] Bret T, Hofmann T and Edinger K 2014 Industrial perspective on focused electron beam-induced processes *Appl. Phys. A Mater. Sci. Process.* **117** 1607–14

[17] Sangiao S, Martín S, González-Orive A, Magén C, Low P J, De Teresa J M and Cea P 2017 All-Carbon Electrode Molecular Electronic Devices Based on Langmuir–Blodgett Monolayers *Small* **13** 1603207

[18] Utke I, Hoffmann P, Berger R and Scandella L 2002 High-resolution magnetic Co supertips grown by a focused electron beam *Appl. Phys. Lett.* **80** 4792–4

[19] Pablo-Navarro J, Sanz-Hernández D, Magén C, Fernández-Pacheco A and De Teresa J M 2017 Tuning shape, composition and magnetization of 3D cobalt nanowires grown by focused electron beam induced deposition (FEBID) *J. Phys. D. Appl. Phys.* **50** 1603207

[20] Winkler R, Schmidt F P, Haselmann U, Fowlkes J D, Lewis B B, Kothleitner G, Rack P D and Plank H 2017 Direct-Write 3D Nanoprinting of Plasmonic Structures *ACS Appl. Mater. Interfaces* **9** 8233–40

[21] Shawrav M M, Taus P, Wanzenboeck H D, Schinnerl M, Stöger-Pollach M, Schwarz S, Steiger-Thirsfeld A and Bertagnolli E 2016 Highly conductive and pure gold nanostructures grown by electron beam induced deposition *Sci. Rep.* **6** 34003

[22] Makise K, Mitsuishi K, Shimojo M and Furuya K 2009 A nanosized photodetector fabricated by electron-beam-induced deposition *Nanotechnology* **20** 425305

[23] Kolb F, Schmoltner K, Huth M, Hohenau A, Krenn J, Klug A, List E J W and Plank H 2013 Variable tunneling barriers in FEBID based PtC metal-matrix nanocomposites as a transducing element for humidity sensing *Nanotechnology* **24** 305501

[24] Hirt L, Reiser A, Spolenak R and Zambelli T 2017 Additive Manufacturing of Metal Structures at the Micrometer Scale *Adv. Mater.* **29** 1604211

[25] Huth M, Porrati F and Dobrovolskiy O V. 2018 Focused electron beam induced deposition meets materials science *Microelectron. Eng.* **185**–**186** 9–28

[26] Peinado, P.; Sangiao, S. De Teresa J M 2015 Focused Electron and Ion Beam Induced Deposition on Flexible and Transparent Polycarbonate Substrates *ACS Nano* **9** 6139–46

[27] Choi Y R, Rack P D, Frost B and Joy D C 2007 Effect of electron beam-induced deposition and etching under bias *Scanning* **29** 171–6

[28] Plank H, Gspan C, Dienstleder M, Kothleitner G and Hofer F 2008 The influence of beam defocus on volume growth rates for electron beam induced platinum deposition *Nanotechnology* **19** 485302

[29] De Teresa J M, Cárdoba R, Fernández-Pacheco A, Montero O, Strichovanec P and Ibarra M R 2009 Origin of the difference in the resistivity of as-grown focused-ion- and focused-electron-beam-induced Pt nanodeposits *J. Nanomater.* **2009** 936863

[30] Huth M, Klingenberger D, Grimm C, Porrati F and Sachser R 2009 Conductance regimes of W-based granular metals prepared by electron beam induced deposition *New J. Phys.* **11** 033032

[31] Rao K A G, Nadasen N and Naik V. M. 2013 *Theoretical and numerical analysis of non-conventional systems for generating static electric fields: A monograph* (Strategic Book Publishing)

[32] Fowlkes J D, Randolph S J and Rack P D 2005 Growth and Simulation of High – Aspect Ratio Nanopillars by Primary and Secondary Electron – Induced Deposition *J. Vac. Sci. Technol. B* **23** 2825–32

[33] Smith D A, Fowlkes J D and Rack P D 2007 A nanoscale three-dimensional Monte Carlo simulation of electron-beam-induced deposition with gas dynamics *Nanotechnology* **18** 265308

[34] Arnold G, Timilsina R, Fowlkes J, Orthacker A, Kothleitner G, Rack P D and Plank H 2014 Fundamental resolution limits during electron-induced direct-write synthesis *ACS Appl. Mater. Interfaces* **6** 7380–7

[35] Schmied R, Fowlkes J D, Winkler R, Rack P D and Plank H 2015 Fundamental edge broadening effects during focused electron beam induced nanosynthesis *Beilstein J. Nanotechnol.* **6** 462–71

[36] Orloff J and Swanson L W 1979 An asymmetric electrostatic lens for field-emission microprobe applications *J. Appl. Phys.* **50** 2494–501

[37] Eppink A T J B and Parker D H 1997 Velocity map imaging of ions and electrons using electrostatic lenses: Application in photoelectron and photofragment ion imaging of molecular oxygen *Rev. Sci. Instrum.* **68** 3477–84

[38] Lin Y and Joy D C 2005 A new examination of secondary electron yield data *Surf. Interface Anal.* **37** 895–900

[39] Futamoto M, Hanbucken M, Harland C J, Jones G W and Venables J A 1985 Visualization of submonolayer and surface topography by biassed secondary electron imaging: application to Ag layers on Si and W surfaces *Surf. Sci.* **150** 430–50

[40] Walsh C A 1992 Effect of specimen bias on secondary electron images in the STEM *Ultramicroscopy* **45** 85–93

[41] Everhart T E and Thornley R F M 1960 Wide-band detector for micro-microampere low-energy electron currents *J. Sci. Instrum.* **37** 246–8

[42] Thiel B L, Toth M, Schroemges R P M, Scholtz J J, Van Veen G and Knowles W R 2006 Two-stage gas amplifier for ultrahigh resolution low vacuum scanning electron microscopy *Rev. Sci. Instrum.* **77** 033705

[43] Heerkens C T H, Kamerbeek M J, van Dorp W F, Hagen C W and Hoekstra J 2009 Electron beam induced deposited etch masks *Microelectron. Eng.* **86** 961–4

[44] Utke I, Hoffmann P and Melngailis J 2008 Gas-Assisted Focused Electron Beam and Ion Beam Processing and Fabrication *J. Vac. Sci. & Technol. B Microelectron. Nanom. Struct.* **26** 1197

[45] Chen P, Van Veldhoven E, Sanford C A, Salemink H W M, Maas D J, Smith D A, Rack P D and Alkemade P F A 2010 Nanopillar growth by focused helium ion-beam-induced deposition *Nanotechnology* **21** 455302

[46] Córdoba R, Ibarra A, Mailly D and De Teresa J M 2018 Vertical Growth of Superconducting Crystalline Hollow Nanowires by He^+ Focused Ion Beam Induced Deposition *Nano Lett.* **18** 1379–86

[47] Al Mamoori M K I, Keller L, Pieper J, Barth S, Winkler R, Plank H, Müller J and Huth M 2018 Magnetic characterization of direct-write free-form building blocks for artificial magnetic 3D lattices *Materials (Basel).* **11** 289

[48] Fernández-Pacheco A, Streubel R, Fruchart O, Hertel R, Fischer P and Cowburn R P

2017 Three-dimensional nanomagnetism *Nat. Commun.* **8** 15756

[49] Pablo-Navarro J, Magén C, De Teresa J M 2016 Three-dimensional core-shell ferromagnetic nanowires grown by focused electron beam induced deposition *Nanotechnology* **27** 285302

[50] Kim K S, Zhao Y, Jang H, Lee S Y, Kim J M, Kim K S, Ahn J-H, Kim P, Choi, J Y, Jong B H 2009 Large-scale pattern growth of graphene films for stretchable transparent electrodes *Nature* **457** 706-710

SUPPLEMENTARY FILE

Diameter modulation of 3D nanostructures in Focused Electron Beam Induced Deposition using local electric fields and beam defocus

Javier Pablo-Navarro[1£], Soraya Sangiao[1,2,3£], César Magén[1,2,3] and José María de Teresa[1,2,3*]

[1] Laboratorio de Microscopías Avanzadas (LMA) - Instituto de Nanociencia de Aragón (INA), Universidad de Zaragoza, 50018 Zaragoza, Spain.

[2] Departamento de Física de la Materia Condensada, Universidad de Zaragoza, 50009 Zaragoza, Spain.

[3] Instituto de Ciencia de Materiales de Aragón (ICMA), Universidad de Zaragoza-CSIC, 50009 Zaragoza, Spain.

SUPPLEMENTARY INFORMATION

-In Figure S1, we show that it is not possible to grow 3D nanowires on fully insulating bare substrates made of materials such as MgO (b) or quartz (c), in contrast to the use of amorphous SiO_2 on Si substrate (a), given that, in the latter case, the charge is dissipated through the conductive Si.

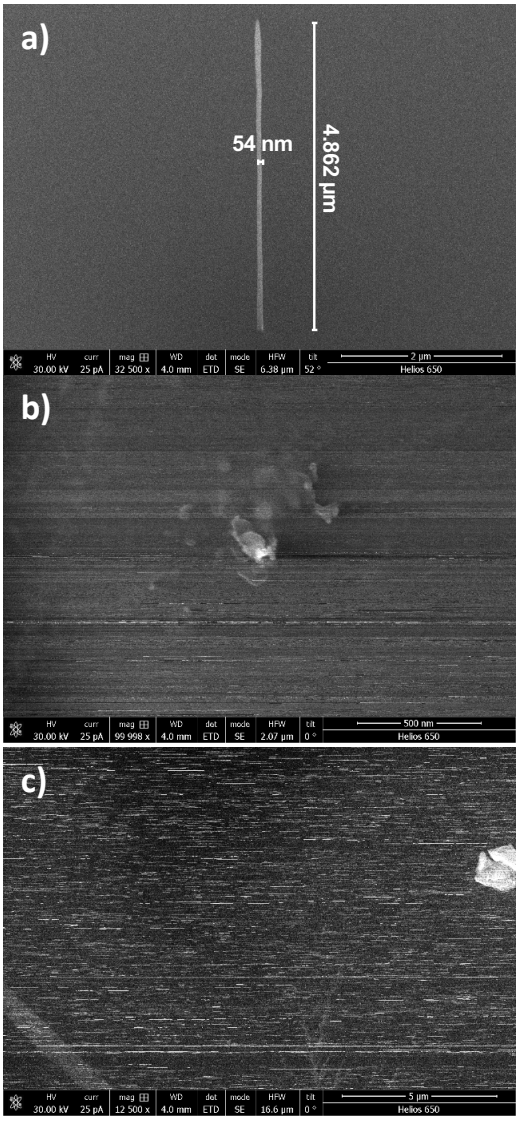

Figure S1. SEM images of 3D Pt-FEBID nanowires grown on the insulating (a) amorphous SiO_2, (b) MgO and (c) quartz substrates. All the deposits were fabricated at 30 kV, 25 pA, with the GIS needle position at x,y,z = 50 µm, and with a deposit time of 211 s. The nanowire only grows on the amorphous SiO_2 substrate because of the underlying conductive Si substrate that is able to dissipate the charge accumulated during growth.

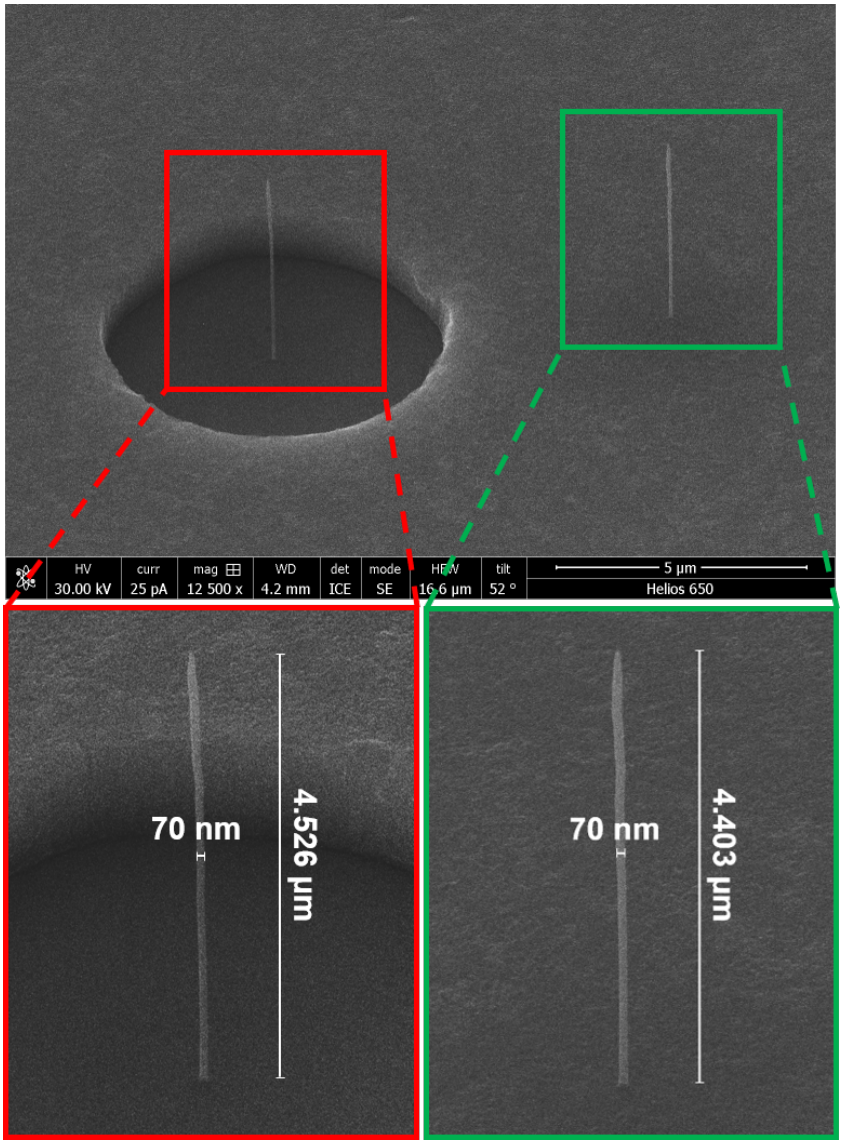

Figure S2. Original SEM micrographs of Figure 2, without artificial colour.

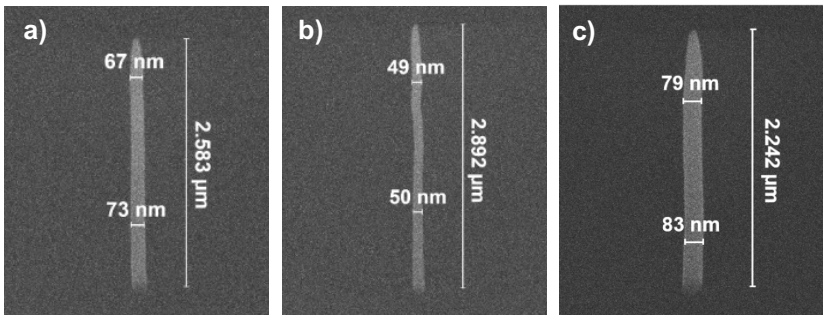

Figure S3. Original SEM micrographs of Figure 4, without artificial colour.

-In Figure S4, we show the growth of W-C nanowires on the *Aragon_Chip*. The results are indicative of diameter modulation (a) and change in the length-to-diameter ratio (b) by application of voltage to the Aragon_Chip, which produces high electric fields on the primary beam and the generated secondary electrons.

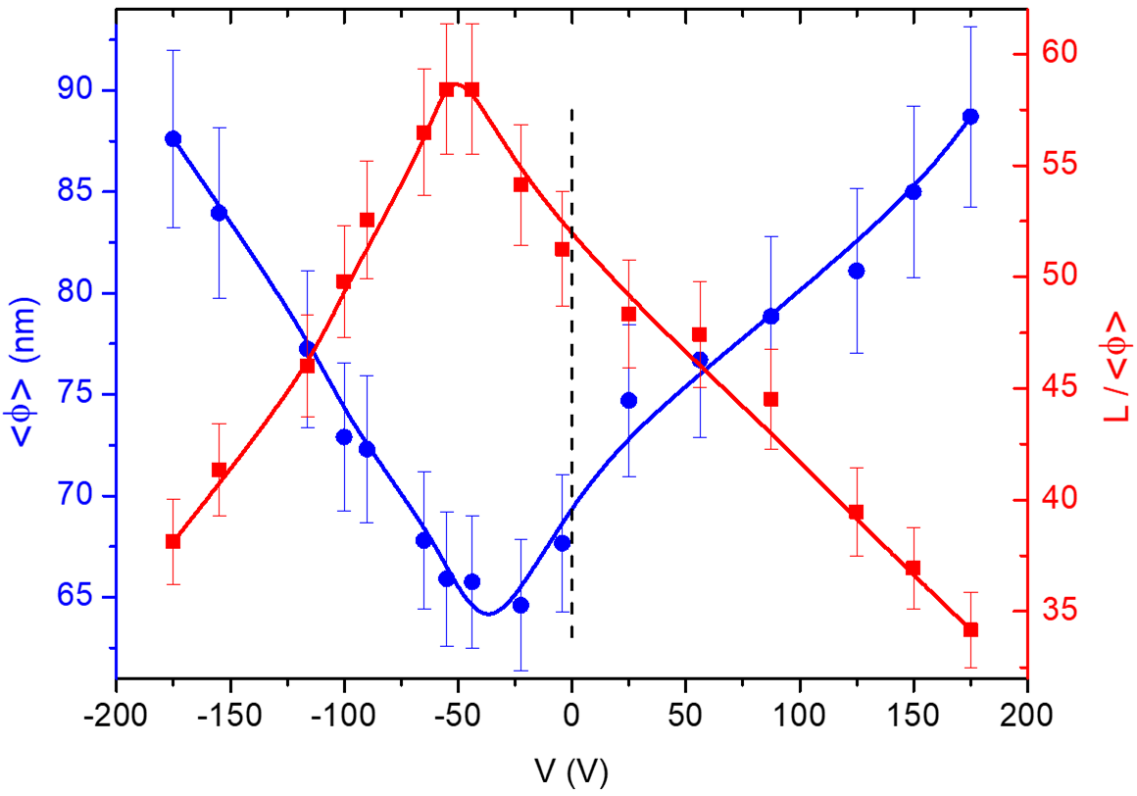

Figure S4. For W-C nanowires grown on SiO_2 for 175 s using the same conditions, dependence of their diameter and the ratio between their length and diameter, with the voltage applied to the perforated copper film. Each data point represents the average value after measurements of several nanowires grown under the same conditions and at various locations in each nanowire.

-In Figure S5, we show SEM micrographs of the same growth area when it is in focus (b) or defocused by +20 μm (a) and -20 μm (c).

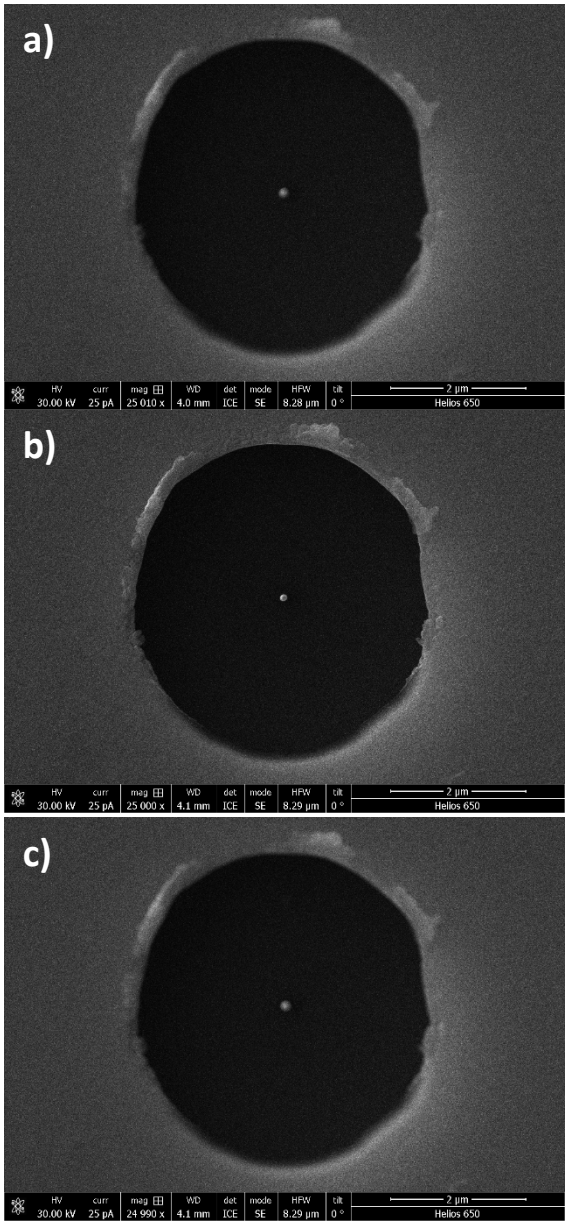

Figure S5. SEM micrographs of a hole of the *Aragon_Chip* with a 3D Pt-FEBID nanowire grown on SiO_2 with the electron beam focused (a) 20 μm above the height of the copper surface, (b) at the height of the copper surface and (c) 20 μm under the height of the copper surface (in all cases there is no voltage applied to the *Aragon_Chip*).

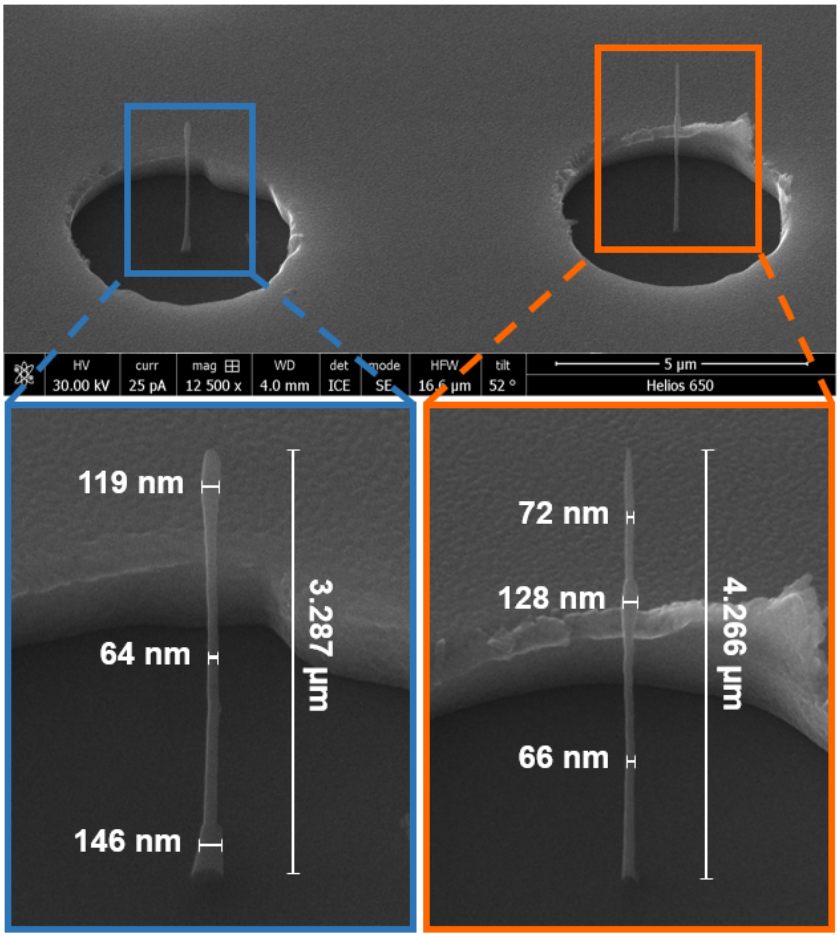

Figure S6. Original SEM micrographs of Figure 7, without artificial colour.

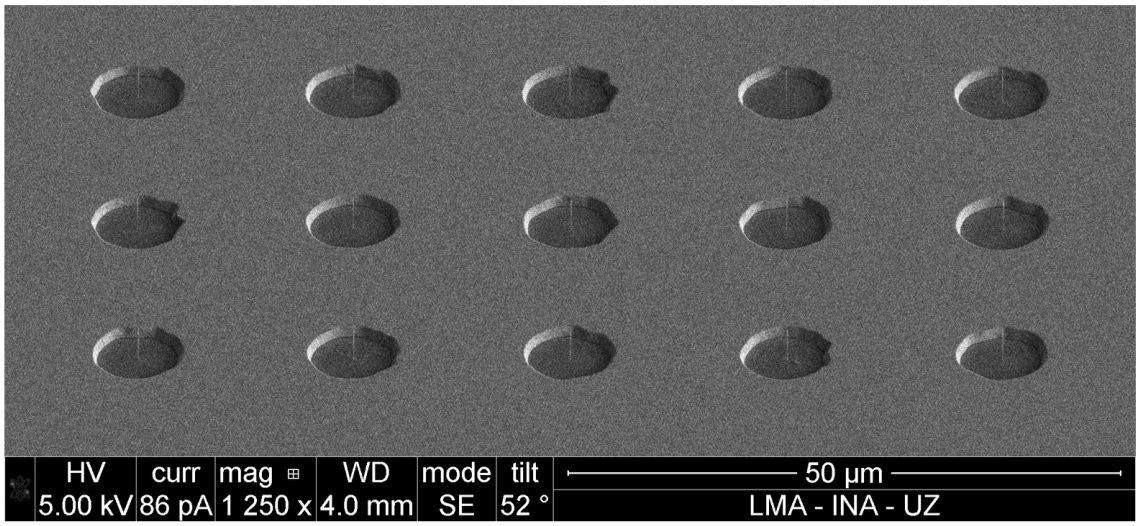

Figure S7. SEM micrograph illustrating a broad view of the Aragon_Chip with 15 grown nanowires.